Nonlinear dynamics of kink-unstable spheromak equilibria

Pablo Luis García-Martínez and Ricardo Farengo

Citation: Physics of Plasmas (1994-present) **16**, 082507 (2009); doi: 10.1063/1.3204639
View online: http://dx.doi.org/10.1063/1.3204639
View Table of Contents: http://scitation.aip.org/content/aip/journal/pop/16/8?ver=pdfcov
Published by the AIP Publishing

Nonlinear dynamics of kink-unstable spheromak equilibria

Pablo Luis García-Martínez[1,2,a)] and Ricardo Farengo[2]
[1]*Consejo Nacional de Investigaciones Científicas y Técnicas (CONICET), Argentina*
[2]*Centro Atómico Bariloche (CNEA) and Instituto Balseiro (UNC-CNEA), San Carlos de Bariloche, RN 8400, Argentina*

(Received 3 June 2009; accepted 6 July 2009; published online 19 August 2009)

The nonlinear evolution of several kink-unstable, force-free equilibria inside a cylindrical flux conserver is studied by solving the nonlinear, three-dimensional, time-dependent equations of resistive magnetohydrodynamics (MHD). The stability properties of the equilibria are controlled by the slope, α, of the linear $\lambda(\psi)$ profile (where $\lambda=\mu_0\mathbf{J}\cdot\mathbf{B}/B^2$ and ψ is the poloidal flux). Very unstable configurations (with α well beyond the stability threshold) are observed to fully relax toward the Taylor state, as predicted by relaxation theory. In contrast, marginally unstable cases undergo only partial relaxation. Since we consider decaying plasmas without open flux (no driving), the partial relaxation process is a result of the dynamics of marginally unstable configurations. The effect of the Lundquist number, S, on a fixed initial condition (a fixed α) is studied. Increasing S leads to a higher level of fluctuations and poloidal flux amplification. However, it is found that, despite the stronger activity, the final level of relaxation is determined only by the initial slope α (for the high S regime considered here). The nonaxisymmetric activity produced by the instability is studied. The relaxation event begins with a dominant $n=1$ kink mode responsible for poloidal flux amplification and ends with a low activity period (of several tens of Alfvén times) which produces a current redistribution process that flattens the λ profile. Finally, the MHD dynamo field is investigated. © *2009 American Institute of Physics*. [DOI: 10.1063/1.3204639]

I. INTRODUCTION

A spheromak is a simply connected confinement configuration in which the magnetic field is produced almost entirely by currents flowing in the plasma.[1,2] Its topological simplicity represents an important advantage from an engineering and economical point of view, but introduces some difficulties related to the sustainment of the configuration against resistive dissipation. Most of the steady-state, driven spheromaks have currents flowing through plasma-facing electrodes, which are orthogonal to the magnetic axis. Magnetic relaxation, which necessarily involves nonaxisymmetric (i.e., three-dimensional) magnetohydrodynamic (MHD) mode activity, drives toroidal current along the magnetic axis. According to the theory of magnetic relaxation, the configuration should relax to a state of minimum magnetic energy subject to the conservation of magnetic helicity, usually called the Taylor state.[3,4] While this theory qualitatively predicts the observed configurations,[5–7] it provides neither an explanation on how the toroidal current is driven, nor the details of the dynamics of the process. Furthermore, the observed configurations, for example, in plasma gun experiments, are not fully relaxed.[5,8] These configurations can be divided into the *central column*, comprising the open flux linked by the electrodes, and the surrounding *annulus*, containing the closed toroidal flux.[6] When the field aligned current in the central column is high, compared with the field aligned current in the annulus, the central column becomes kink unstable.[9] The finite amplitude saturation of this instability produces a rotating helical structure, which increases the current in the annulus through a dynamolike process.[10,11] Measurements of the parallel component of the MHD dynamo field revealed the presence of a single-mode antidynamo process in the central column and a turbulent dynamo process in the annulus.[12]

Many theoretical efforts have been devoted to study this current drive process. The conditions for the onset of the $n=1$ kink instability, in terms of the $\lambda(\psi)$ profile (where $\lambda=\mu_0\mathbf{J}\cdot\mathbf{B}/B^2$ and ψ is the poloidal flux), have been determined using linear ideal MHD stability codes.[5,9,13] Nonlinear studies of spheromak relaxation have also been performed using numerical simulations. Katayama and Katsurai[14] simulated a decaying spheromak in a cylindrical flux conserver for several q profiles and observed the growth of an $n=1$ mode and poloidal flux generation for the hollow λ profile situation (see Sec. II B). Their study was restricted to unstable modes with relatively high growth rates (larger than $0.01/\tau_A$, where τ_A is the Alfvén time) due to computer limitations and all the final states obtained in their simulations were very similar to the Taylor state. The evolution of an unstable spheromak equilibrium in a "bowtie" flux conserver was simulated by Izzo and Jarboe.[15] Using the same initial condition, they varied the Lundquist number over one order of magnitude and identified the minimum value needed for poloidal flux generation. Formation and sustainment in both a cylindrical "flux core" configuration and a coaxial gun were studied by Sovinec *et al.*[16]

In this paper we consider the evolution of several kink-unstable force-free equilibria, inside a cylindrical flux conserver, with neither open flux nor sustainment, using the zero-β resistive MHD model.[15,16] Unlike Ref. 15, which fo-

a)Electronic mail: pablogm@cab.cnea.gov.ar.

cused on the effect of the Lundquist number on the evolution of the same unstable (to the $n=1$ kink mode) initial condition, we study the evolution of equilibria with different λ profiles (ranging from stable to well beyond the stability threshold) and different Lundquist numbers. In addition, we analyze the evolution of the MHD dynamo field and its spatial structure in the poloidal plane.

The stability to the $n=1$ kink mode is determined by the slope of the linear $\lambda(\psi)$ profile.[5,13] By varying this parameter we are able to find different behaviors. Initial equilibria with steep slopes, well beyond the instability threshold, are observed to develop a high level of nonaxisymmetric fluctuations and relax completely to a Taylor state, as predicted by relaxation theory. In contrast, marginally unstable equilibria undergo only partial relaxation (Sec. III A). Partially relaxed configurations observed in experiments are usually regarded as the result of a competition between sustainment and relaxation.[11] In this work we show that partial relaxation may take place as a result of the dynamics of marginally unstable equilibria, even in the absence of open field lines and sustainment. In agreement with previous numerical results,[15] we observe that, when the Lundquist number is increased for a fixed value of α, more activity and more poloidal flux amplification take place. However, our results show that the level of relaxation (see Sec. III A) does not change when S increases. In this system, the level of relaxation produced by the kink instability evolution is dictated by the initial slope α.

The initial linear phase of the instability, the exponential growth of the $n=1$ kink eigenmode, is recovered. We show that, in marginally unstable cases, the initial perturbation must be similar to the appropriate eigenmode in order to quickly activate the instability. Our study of the fluctuations produced by the instability shows that the $n=1$ kink mode is dominant during poloidal flux amplification (in agreement with experimental observations[10,11]). After saturation, the fluctuations decrease fast, down to a small level. In spite of their small value, these remaining fluctuations produce a significant current redistribution process that flattens the λ profile. This final stage of the relaxations process lasts several tens of Alfvén times.

We also study the MHD dynamo produced by the fluctuations (Sec. III D). The distribution of the parallel component of the dynamo field, in the poloidal plane, shows a strong antidynamo process concentrated near the geometric axis (in the outer flux surfaces) and a positive dynamo near the magnetic axis. From the comparison of the dynamo level obtained at the magnetic axis, in several cases with different initial slopes and different Lundquist numbers, we find that the dynamo level is directly related to the $n=1$ fluctuation level, regardless of α and S.

The rest of the paper is organized as follows. In Sec. II, the physics model and the details of the numerical scheme employed are presented. We discuss some aspects regarding the perfectly conducting boundary condition applied at the cylinder walls (Sec. II A). The initial condition is described in Sec. II B. There, we describe a simple strategy to obtain a numerical approximation to the $n=1$ kink eigenmode, suitably to activate the instability in the marginally unstable cases. The results are presented and discussed in Sec. III. Finally, a summary and the conclusions are presented in Sec. IV.

II. COMPUTATIONAL APPROACH

Simulations in this study are performed with the Versatile Advection Code,[17] a numerical code originally developed for the astrophysics community, in which several numerical methods for solving the compressible hydrodynamic and MHD equations are implemented. In particular, this code can be used to solve the isothermal resistive MHD model, which is the one employed in this work. The isothermal MHD equations are nondimensionalized using a length scale a (the chamber radius), a density scale ρ_0, and a magnetic field scale B_0. With these quantities we can define the Alfvén velocity scale $c_A=B_0/\sqrt{\mu_0\rho_0}$, the Alfvén time $\tau_A=a/c_A$, and the current scale $J_0=B_0/a\mu_0$. The resulting dimensionless equations are

$$\frac{\partial\rho}{\partial t}+\nabla\cdot(\rho\mathbf{u})=0, \tag{1}$$

$$\frac{\partial\mathbf{u}}{\partial t}+\mathbf{u}\cdot\nabla\mathbf{u}+\beta\frac{\nabla p}{\rho}=\frac{\mathbf{J}\times\mathbf{B}}{\rho}+\tilde{\nu}\nabla\cdot\Pi, \tag{2}$$

$$\frac{\partial\mathbf{B}}{\partial t}+\nabla\times\mathbf{E}=0, \tag{3}$$

where $\mathbf{J}=\nabla\times\mathbf{B}$, $\mathbf{E}=-\mathbf{u}\times\mathbf{B}+\tilde{\eta}\mathbf{J}$, $\Pi=(\nabla\mathbf{u}+\nabla\mathbf{u}^T)-(2/3)\times(\nabla\cdot\mathbf{u})$, and $p=c_s^2\rho$ (isothermal assumption), where c_s is the sound speed.

The parameter $\beta=\mu_0 p_0/B_0^2=c_s^2/c_A^2$ (the pressure scale p_0 may be derived from ρ_0, as $p_0=c_s^2\rho_0$) quantifies the relative importance of hydrodynamics forces (coming from pressure gradients) and magnetic forces (Lorenz's force). Spheromaks are low β plasmas so, to first order approximation, forces due to hydrodynamic pressure gradients may be ignored. For this reason, we do not advance the continuity equation, Eq. (1). Since the initial condition has uniform density (and consequently pressure), the pressure forces vanish in our simulations. This simplification is usually referred to as the zero-β (or zero-pressure) approximation and is widely used when modeling low-β plasmas.[15,16]

The parameter $\tilde{\nu}=\nu/(ac_A)$ is the dimensionless kinematic viscosity and $\tilde{\eta}=\eta/(\mu_0 a c_A)$ is the dimensionless resistivity. Both are considered spatially uniform. In this work we use $\beta=0$ (uniform density), $P_m=\tilde{\nu}/\tilde{\eta}=1$ (magnetic Prandtl), and three values for $\tilde{\eta}$, 2×10^{-5}, 5×10^{-5}, and 10^{-4}. The parameter $\tilde{\eta}$ may also be interpreted as the ratio of two time scales: the Alfvén time (representative of MHD wave propagation) and a resistive time. Although it is common to define the Lundquist number ($S=\tau_r/\tau_A$) as the inverse of $\tilde{\eta}$,[16] we employ a more appropriate choice for the resistive time scale:[15] $\tau_r=\mu_0/(\eta\lambda_1^2)$, where λ_1^{-1} is the length scale derived from the force-free spheromak relation $\nabla\times\mathbf{B}=\lambda\mathbf{B}$, which turns out to be, for a cylindrical flux conserver of radius a and height h,

$$\lambda_1 = \sqrt{\left(\frac{x_{11}}{a}\right)^2 + \left(\frac{\pi}{h}\right)^2}, \tag{4}$$

where x_{11} is the first zero of the Bessel function J_1. With this definition, the Lundquist numbers obtained for the different values of $\tilde{\eta}$ used are 2036, 814, and 407, respectively (considering $a=h=1$, which gives $\lambda_1=4.955$).

The system of partial differential equations that composes the physics model is solved in a uniform Cartesian grid, with $N_x \times N_y \times N_z = 100 \times 100 \times 50$. In order to simplify the analysis of the results, we define a poloidal grid (with $N_r = 50 \times N_z = 50$), where we store the Fourier coefficients of the toroidal decomposition of $\mathbf{u}$, $\mathbf{B}$, and $\mathbf{J}$, so that we have available the axisymmetric $(n=0)$ and nonaxisymmetric $(n=1,2,\cdots)$ components of the solution. The numerical scheme we use is a total variation diminishing Roe's approximate Riemann solver, together with the projection method, which maintains the $\nabla \cdot \mathbf{B}=0$ constraint numerically.[18] This numerical scheme does not require diffusive terms in the governing equations for numerical stability. Like classical upwind methods, the discretization errors of this scheme introduce a stabilizing numerical dissipation. The amount of numerical dissipation introduced is proportional to the grid refinement. Since we do not want to rely on this numerical dissipation, we verify that it is lower than the physical dissipation that one can control (by imposing high values of $\tilde{\eta}$ and $\tilde{\nu}$). In order to check that the lowest value of $\tilde{\eta}$ used led to a physical dissipation well above the numerical dissipation due to the grid employed, we used the following procedure. We selected the most unstable case analyzed in this work (that with $\alpha=-0.8$, see Sec. II B). We performed several runs of this case varying $\tilde{\eta}$. Then we performed the same runs changing only the grid size: We used double resolution in each spatial direction ($200 \times 200 \times 100$ grid points). We compared the results, in terms of the flux amplification obtained, which is known to be a quantity very sensitive to the dissipation coefficients.[15] The difference in the flux amplification obtained with the two grids in this case ($\alpha=-0.8$), with $\tilde{\eta}=2\times10^{-5}$, has a peak of 2% during the period maximum activity. We note that even when this difference increases as $\tilde{\eta}$ is set to lower values, the qualitative aspects of the two evolutions are the same.

A. Boundary conditions and relaxed state

The fixed physical domain considered in this work is a cylindrical flux conserver of radius $a=1$ and elongation $h/a=1$. Boundary conditions at the flux conserver walls are imposed using a simple high-order boundary treatment for Cartesian grids methods.[19] The usual perfectly conducting wall conditions employed are $(\mathbf{B}\cdot\hat{\mathbf{n}})|_{\partial\Omega}=0$ and $(\mathbf{J}\times\hat{\mathbf{n}})|_{\partial\Omega}=0$, together with the nonslip condition $\mathbf{u}|_{\partial\Omega}=0$.[14,15] The condition $(\mathbf{J}\times\hat{\mathbf{n}})|_{\partial\Omega}=0$ has to be satisfied, because otherwise a net electric field, coming from the term $\eta\mathbf{J}$ in Ohm's law, is created along the walls.[16] Note that this condition forces $\lambda|_{\partial\Omega}=0$.

The force-free equilibria used as initial conditions have a linear $\lambda(\psi)$ profile that does not vanish at the wall ($\psi=0$). The slope, α, of this linear profile controls the stability to the kink mode. Unstable equilibria should relax to a Taylor state, which is given by the eigenfunction of $\nabla\times\mathbf{B}=\lambda\mathbf{B}$, $(\mathbf{B}\cdot\hat{\mathbf{n}})|_{\partial\Omega}=0$, associated with the lowest eigenvalue $\lambda=\lambda_1$, given by Eq. (4) in our geometry. This preferred, reference state has a uniform λ ($\alpha=0$), which does not vanish at the walls.

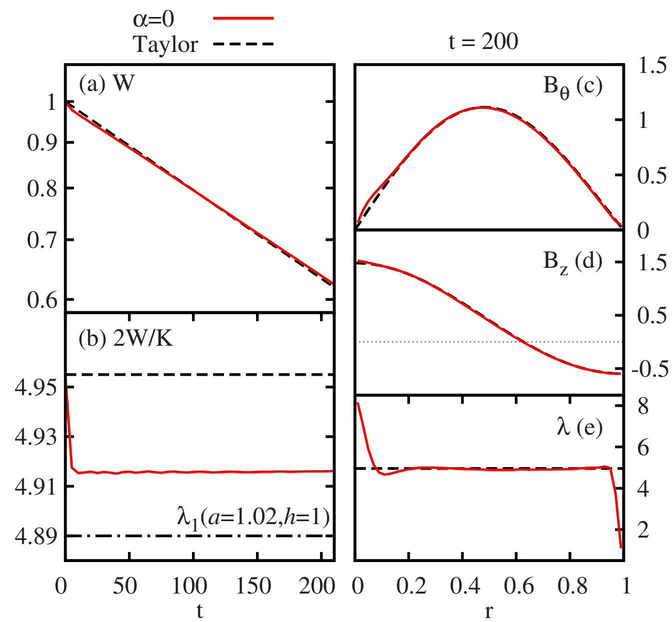

FIG. 1. (Color online) Comparison between the numerical $\alpha=0$ case and the analytic Taylor state. Magnetic energy decay (a). Time is given in Alfvén times. Evolution of the ratio 2 W/K (b). Radial profiles at $z=0.5$ of the toroidal (c) and axial (d) components of the magnetic field and λ (e).

Thus, it is of interest to analyze the properties of the relaxed configuration allowed by our boundary conditions, toward which unstable equilibria are supposed to evolve, compared with the analytic Taylor state. To this end we use the Taylor state as initial condition and run the code during 250 Alfvén times. The results of this run will be taken as the reference relaxed state, when comparing with the unstable cases, and referred to as the $\alpha=0$ case. Figure 1 compares several aspects of the $\alpha=0$ case with the analytic Taylor state. First, we can see that the exponential resistive energy decay of the Taylor state $[W_{\text{Taylor}} \propto \exp(-2\eta\lambda_1^2 t)]$ is recovered [Fig. 1(a)]. Second, in Fig. 1(b), it is observed that the relation between the magnetic energy W and the magnetic helicity K adopts a constant value very close to $\lambda_1/2$ ($\lambda_1=2$ W/K in the Taylor state). The deviation of 2 W/K [due to a small initial drop in W, visible in Fig. 1(a)] from its theoretical value comes from our discrete numerical representation. Note that the value of λ_1 for a cylinder of radius $\tilde{a}=1+0.02$ (where 0.02 is our grid spacing) falls below the value of 2 W/K of the $\alpha=0$ case [Fig. 1(b)]. Third, the radial profiles of B_θ and B_z at $z=0.5$ (cylinder midheight) and $t=200$ of the $\alpha=0$ case present only small deviations from the analytic profiles of the Taylor state [Figs. 1(c) and 1(d)]. Finally, the radial profile of λ, at $z=0.5$ and $t=200$, clearly shows the effect of the condition $\lambda|_{\partial\Omega}=0$ [Fig. 1(e)] and also shows a rise in λ near the geometric axis [consistent with the small "bump" near $r=0$, observed in Fig. 1(c)].

The λ values in the poloidal plane are shown in Fig.

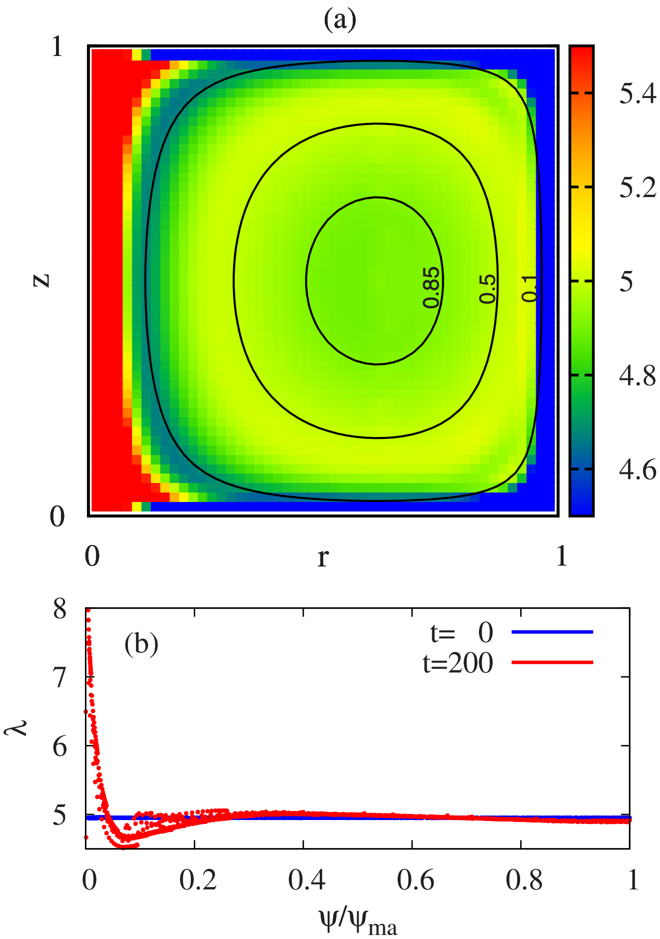

FIG. 2. (Color online) λ in the poloidal plane at $t=200\tau_A$ (a). Black curves indicate contours of $\tilde{\psi}$. $\lambda(\tilde{\psi})$ profile (b).

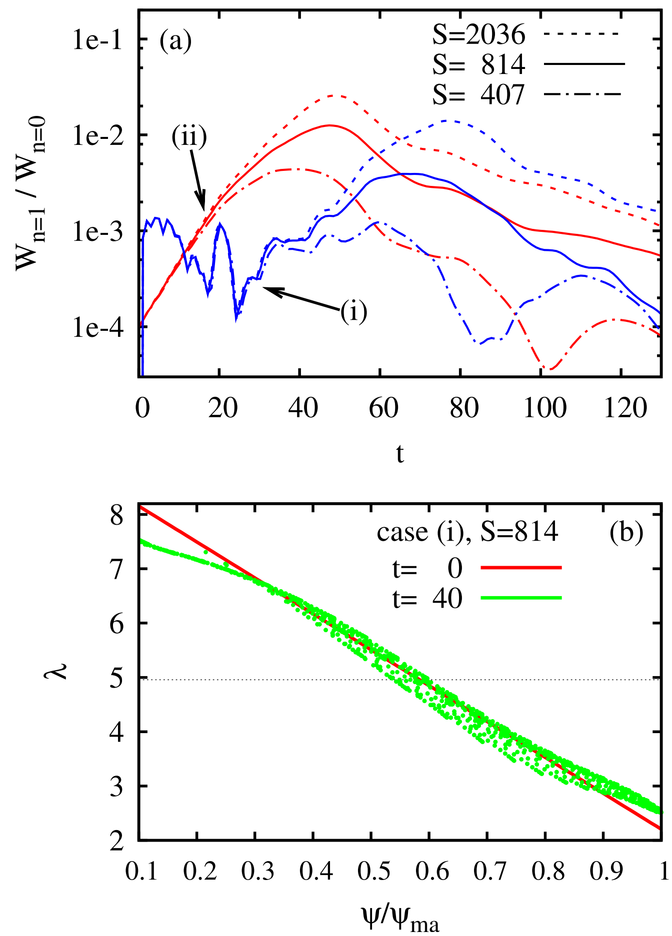

FIG. 3. (Color online) Evolution of the magnetic energy of the $n=1$ component of the solution (relative to the $n=0$ component) for the case $\alpha=-0.6$ (a). In (i), an arbitrary $n=1$ perturbation is added to the velocity field. In (ii), the kink eigenmode is used. $\lambda(\psi)$ profile at $t=0$ and $t=40$, for the case (i) with $S=814$ (b).

2(a), together with three contours of constant normalized poloidal flux $\tilde{\psi}=\psi/\psi_{\mathrm{ma}}$, where ψ_{ma} is the poloidal flux at the magnetic axis. A convenient way of analyzing the values of λ consists in using $\tilde{\psi}$ as a coordinate. This may be done by plotting the pair of values (ψ_{ij},λ_{ij}), obtained at each grid point ij of the poloidal plane, in the λ-$\tilde{\psi}$ space [Fig. 2(b)]. Using $\tilde{\psi}$ as a coordinate for λ is only strictly valid when $\mathbf{J}\times\mathbf{B}=0$. While the initial and final states considered in the next section satisfy (numerically) this condition, intermediate states with MHD activity present do not. However, we can still make this plot at any time and check that, when the configuration is near a MHD equilibrium, the (ψ_{ij},λ_{ij}) points concentrate into a single line. For the $\alpha=0$ case, we observe, in Fig. 2, that the deviation from the uniform λ profile introduced by the numerical boundary conditions only affects the outer flux surfaces, where $\mathbf{J}\times\hat{\mathbf{n}}\sim 0$ and $\mathbf{B}\cdot\hat{\mathbf{n}}\sim 0$, so the condition $\mathbf{J}\parallel\mathbf{B}$ does not hold exactly.

In summary, we checked that the numerical relaxed state compatible with the grid and boundary conditions used in this work is very similar to the analytic Taylor state and reproduces four important properties of it: (i) the resistive decay rate, (ii) the relation between W and K (within the numerical accuracy), (iii) the spatial $\mathbf{B}$ profiles, and (iv) the uniform $\lambda(\tilde{\psi})$ profile (in the inner flux surfaces, away from the condition $\lambda|_{\partial\Omega}=0$).

B. Initial condition and initial perturbation

The initial condition is an axisymmetric force-free ($\mathbf{J}\times\mathbf{B}=0$), pure magnetic ($\mathbf{u}=0$) state. When the magnetic field is axisymmetric, the poloidal flux ψ acts as a stream function for the poloidal magnetic field and the force-free condition may be expressed in terms of the Grad–Shafranov equation for ψ,

$$\Delta^*\psi+\lambda(\psi)\int_0^{\psi}\lambda(\hat{\psi})d\hat{\psi}=0, \tag{5}$$

where $\Delta^*=(\partial^2/\partial r^2)-(1/r)(\partial/\partial r)+(\partial^2/\partial z^2)$. The special case $\lambda(\psi)=\lambda_1$ corresponds to the Taylor state. Experimental observations showed that a better approximation, than the Taylor state, for laboratory spheromaks may be obtained introducing the linear relationship,

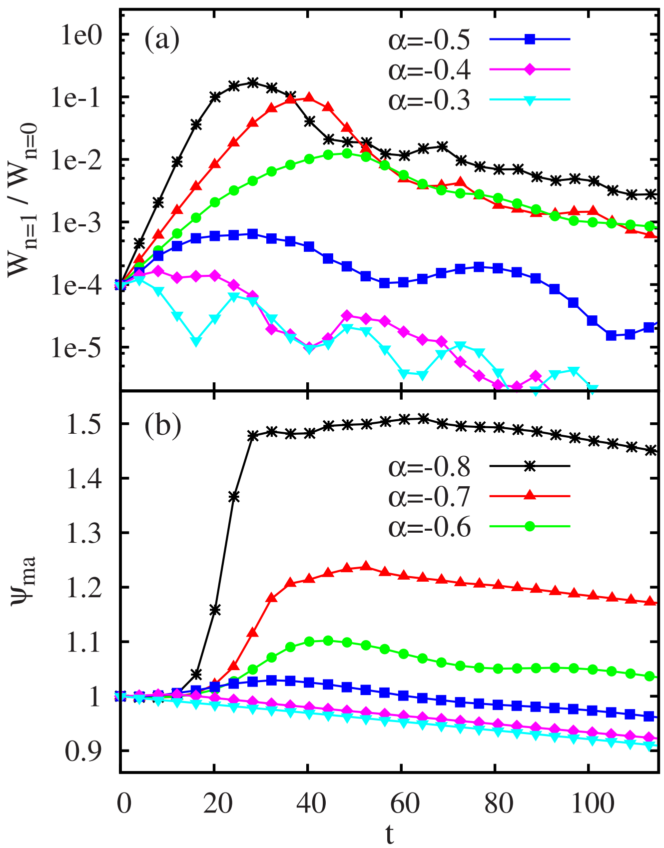

FIG. 4. (Color online) Evolution of the $n=1$ magnetic energy (a) and poloidal flux (b) for different α values and $S=814$.

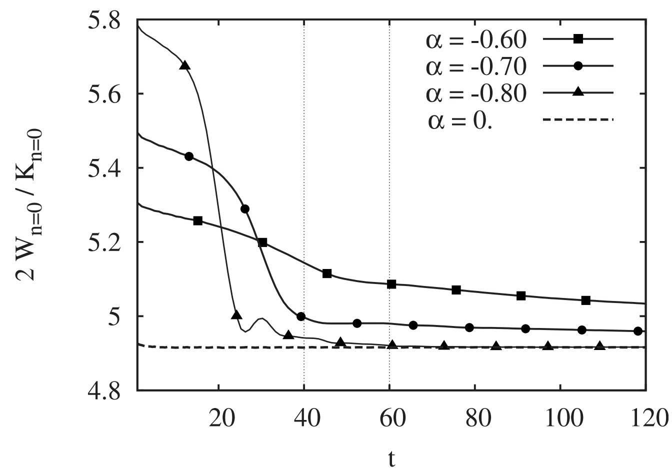

FIG. 5. The $n=0$ magnetic energy ($W_{n=0}$) relative to the $n=0$ magnetic helicity $K_{n=0}$. The lowest value allowed (that of the $\alpha=0$ case) is only achieved by the most unstable case $\alpha=-0.8$.

$$\lambda(\psi) = \bar{\lambda}[1 + \alpha(2\tilde{\psi} - 1)], \tag{6}$$

into Eq. (5). The resulting nonlinear Grad–Shafranov equation may be solved using a quasilinear technique.[20] Note that the normalization factor for ψ is ψ_{ma}, which is a result of the computation. Therefore, one must fix the value of α and iterate over $\bar{\lambda}$ until the solution is equal to one at the magnetic axis.

The sign of the slope α determines whether the current profile is hollow (negative α) or peaked (positive α). Hollow current profiles are representative of the sustainment phase of helicity-injected spheromaks, while peaked current profiles approximate the magnetic configurations observed during spheromak decay.[5] Results of the linear ideal MHD stability analysis show that this type of configurations becomes unstable to an $n=1$ kink mode when α is below -0.4.[5,13] In Sec. III we study the nonlinear evolution of magnetic configurations representative of driven spheromaks, i.e., solutions to Eq. (5), using the linear $\lambda(\psi)$ profile (6), with $\alpha<0$. Each run is characterized by the slope α of its initial condition and the Lundquist number S (407, 814, or 2036).

Before analyzing the simulation results we consider some aspects related to the initial perturbation required to activate the dynamics. When the evolution of unstable equilibria well beyond the stability boundary is considered ($\alpha=-0.8$, for instance), the unstable modes grow immediately regardless of the small perturbation added to the equilibrium. The behavior is different for less unstable cases, near the stability boundary. For example, we consider the evolution of the case with initial slope $\alpha=-0.6$. In Fig. 3, the curves labeled (i) show the evolution of the magnetic energy of the $n=1$ component of the solution (relative to the $n=0$ component) for this case, for different Lundquist numbers. In this case, a small perturbation to the axial component of the velocity (u_z), having toroidal wavenumber $n=1$ and an energy $W_\delta \sim 10^{-3} \times W_0$, is introduced ($W_0$ is the initial magnetic energy). We observe that the instability is triggered after 40 Alfvén times, independently of the Lundquist number. During this period the resistive decay affects the initial $\lambda(\psi)$ profile [Fig. 3(b)], changing the stability properties of the configuration. For this reason, the growth rates obtained for the different values of S are different (note that in the $S=407$ case, the instability disappears). This delay in the onset of the instability growth has been observed in previous studies.[15]

Since sustained spheromaks are supposed to operate near the stability threshold, it is of interest to study the evolution of marginally unstable equilibria as accurately as possible. To that end we employ the following strategy. We take the $n=1$ component (velocity and magnetic field) of the solution (i) at $t=60$, when the instability is active [Fig. 3(a), curve (i)], this component should resemble the kink eigenmode. We multiply this component by a suitable constant, in order to obtain a new $n=1$ perturbation with $W_\delta=10^{-4}W_0$. Using this perturbation, the new computed evolution exhibits a much shorter period preceding the instability growth. Repeating once more this process, we obtain the curves (ii) in Fig. 3(a). In this case, where the perturbation is similar to the kink eigenmode, the exponential growth of the instability is recovered, despite the energy of the perturbation being smaller than in case (i). Furthermore, we see that the growth rate, during the linear phase of the instability, is the same for all the values of S considered.

This example reveals the importance of using a perturbation similar to the appropriate eigenmode of the instability that is being studied. The perturbations used in all the computations presented in Sec. III are obtained in the following

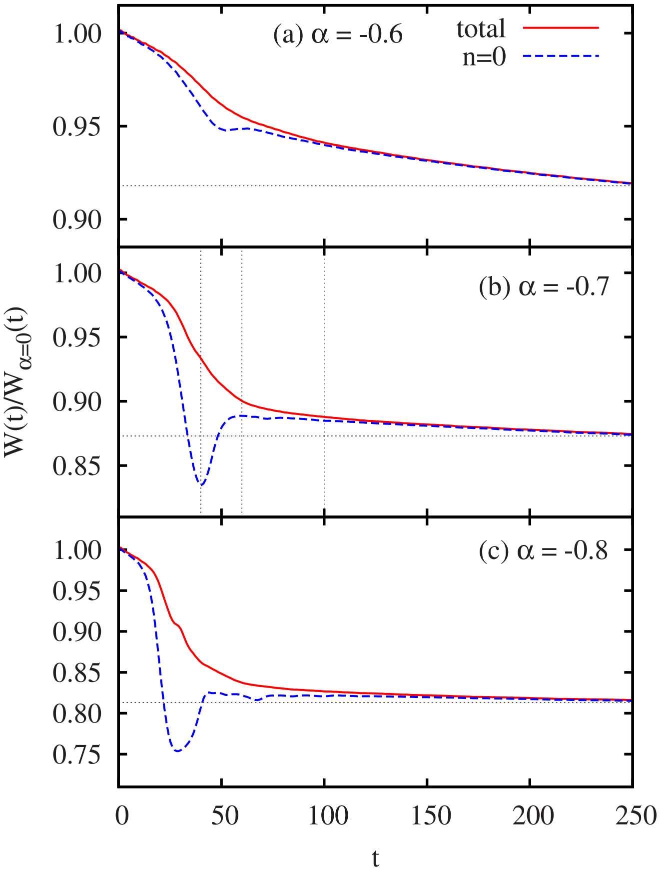

FIG. 6. (Color online) Total and $n=0$ magnetic energy relative to the magnetic energy of the $\alpha=0$ case (normalized) for three unstable cases. After the relaxation event, only the case $\alpha=-0.8$ shows the same resistive decay rate that the relaxed state.

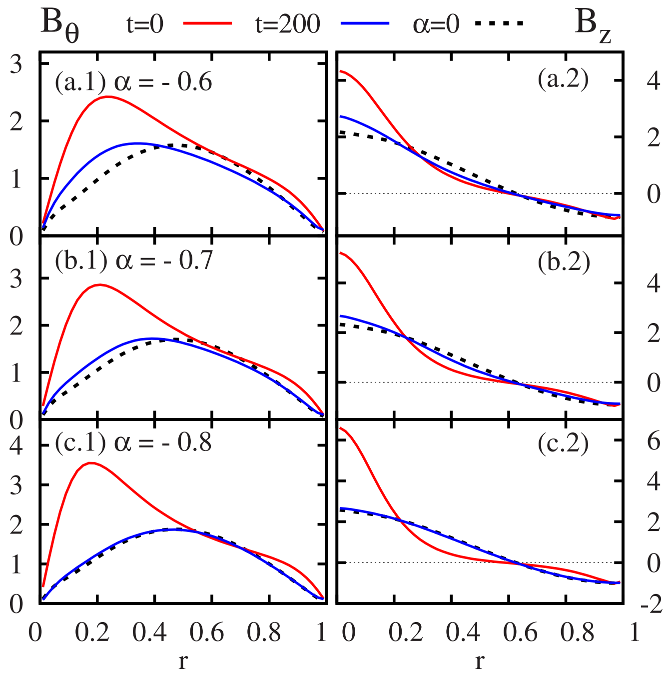

FIG. 7. (Color online) Initial and final radial profiles (at $z=0.5$) of the toroidal and axial components of the magnetic field. The corresponding profiles (at $t=200$) of the $\alpha=0$ case (normalized to obtain the same magnetic energy in each case) are also shown.

way. To each initial condition, we add the eigenmode of the $\alpha=-0.6$ case, calculated above (rescaled to $W_\delta=10^{-4}W_0$). We run the code during ten Alfvén times, take the $n=1$ component and rescale it to obtain $W_\delta=10^{-4}W_0$.

III. RESULTS AND DISCUSSION

The magnetic energy of the $n=1$ component and the poloidal flux at the magnetic axis (ψ_{ma}) obtained for several α values and $S=814$ are shown in Fig. 4. For the unstable cases the exponential growth of the $n=1$ mode during the linear phase of the instability ($t<15$) is recovered. Our results are in good agreement with the calculations of the ideal MHD stability to the $n=1$ mode, using linear ideal MHD codes,[13] which indicate that this mode becomes marginally unstable for $\alpha\sim-0.4$. In the cases with $\alpha\leq-0.5$ the amplification of the poloidal flux is observed ($20\lesssim t\lesssim 40$). The development of the kink instability and its nonlinear saturation are related to the tendency of the plasma to relax toward a state with less magnetic energy and almost the same helicity. In spheromaks, magnetic relaxation brings about the desired effect of toroidal current drive, via a MHD dynamo process. We now turn to study the magnetic relaxation produced by the evolution of the $n=1$ kink instability (Sec. III A) and the effect of the nonaxisymmetric modes on the λ profile (Sec. III B). We also discuss the effect of the resistivity on the dynamics (Sec. III C). Finally, the MHD dynamo produced by the relaxation process is studied (Sec. III D).

A. Magnetic relaxation

Three unstable cases ($\alpha=-0.6,-0.7,-0.8$) are compared with the reference, $\alpha=0$, case. Figure 5 shows the evolution of the ratio $2W_{n=0}/K_{n=0}$ (where K is the magnetic helicity) for the cases $\alpha=0,-0.6,-0.7,-0.8$ ($S=814$). We find that only the more unstable case, $\alpha=-0.8$, dissipates enough energy, relative to helicity, to reach a completely relaxed state. The total and $n=0$ magnetic energy, relative to the magnetic energy of the $\alpha=0$ case (normalized to its initial value), for these three cases is shown in Fig. 6. The more unstable cases exhibit more nonaxisymmetric activity and more energy dissipation during relaxation. At large times ($t>150$) the axisymmetry is recovered in all the cases. The decay rate of the final axisymmetric configuration is smaller for the more unstable cases in which more activity has taken place, in particular, the case $\alpha=-0.8$ finishes with a decay rate very similar to that of the $\alpha=0$ case [an almost horizontal line in Fig. 6(c), $t>150$]. The initial and final radial profiles, at $z=0.5$, of the toroidal and axial components of the magnetic field are shown in Fig. 7. From the comparison of these profiles with the reference $\alpha=0$ case (which is very close to the Taylor state, see Sec. II A), we confirm the picture suggested by Figs. 5 and 6: The level of relaxation achieved depends on the initial slope α and only very unstable cases (those with $\alpha\leq-0.8$, in this case) undergo a complete relaxation. The initial and final $\lambda(\psi)$ profiles for the three cases, shown in Fig. 8, confirm this behavior. When the initial $\lambda(\psi)$ profile is steeper, the final λ profile is closer to the uniform λ state.

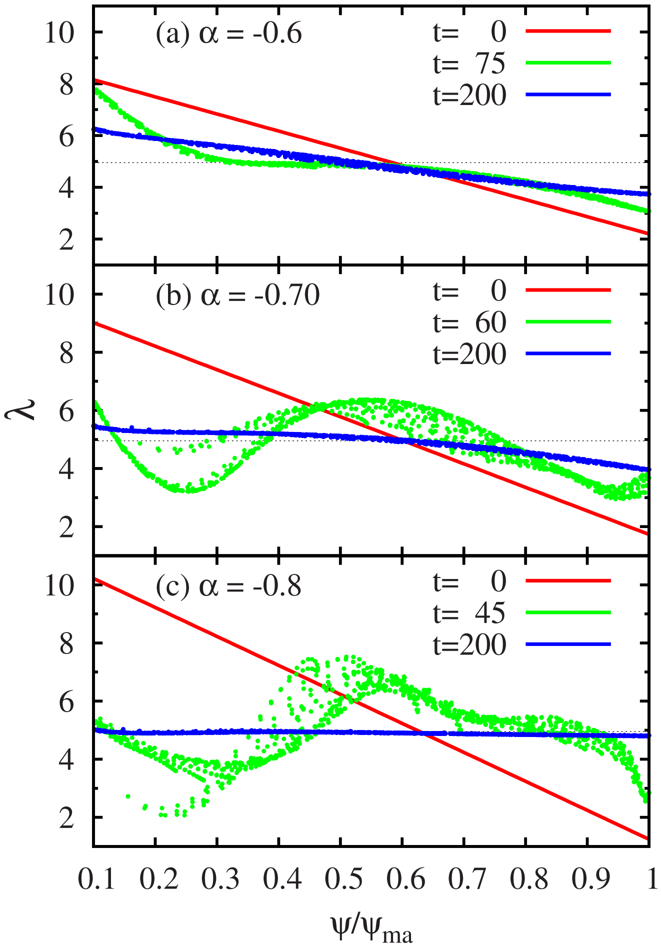

FIG. 8. (Color online) $\lambda(\tilde{\psi})$ profiles at several times for the $\alpha=-0.6$, -0.7, and -0.8 cases ($S=814$).

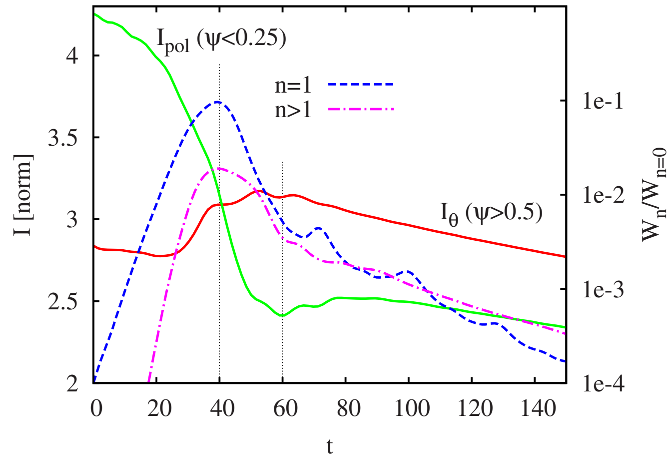

FIG. 9. (Color online) Evolution of the poloidal and toroidal currents in the outer ($\tilde{\psi}<0.25$) and in the internal ($\tilde{\psi}>0.5$) flux surfaces, respectively (solid lines), for the $\alpha=-0.7$, $S=814$ case. Energy of the $n=1$ and $n>1$ modes for the same case (broken lines).

B. Activity during magnetic relaxation

The mechanism underlying the magnetic relaxation (complete or partial, for marginally stable cases) of unstable configurations is the MHD mode activity induced by the instability. It has been determined experimentally that the $n=1$ kink instability is the source of poloidal flux amplification.[11] Our results agree with that observation. In Fig. 4 it is observed that the poloidal flux amplification takes place a few Alfvén times before the instability saturation. The fact that the $n=1$ activity is dominant during this period is shown in Fig. 9, for the particular case $\alpha=-0.7$, $S=814$.

The poloidal flux amplification produced by the kink instability is associated with a toroidal current drive process, in the inner flux surfaces. In many helicity-injected devices, a poloidal current is electrostatically driven along the open field lines (the column) and the system relies on the kink instability to drive toroidal current in the closed flux region (the annulus).[12] Although in our case (no open flux) the separation between column and annulus is somewhat arbitrary, it is clear that the qualitative behavior of cases with open flux is reproduced. The conversion from poloidal current in the central column into toroidal current in the annulus is shown in Fig. 9. In this figure, I_{pol} is defined as the integral of J_z in a circle centered at the geometric axis and $z=0.5$, with radius r_{col}, where $\tilde{\psi}(r_{col},z=0.5,t=0)=0.25$. The toroidal current in the annulus, I_θ, is the integral of J_θ over all the points (r_{an},z_{an}) in the poloidal plane that satisfy $\tilde{\psi}(r_{an},z_{an},t=0)>0.5$.

Note that the poloidal flux amplification and the toroidal current drive process produced by the relaxation take place before instability saturation (at $t\sim 40$, for the $\alpha=-0.7$ case, for example). There are other signatures of relaxation that

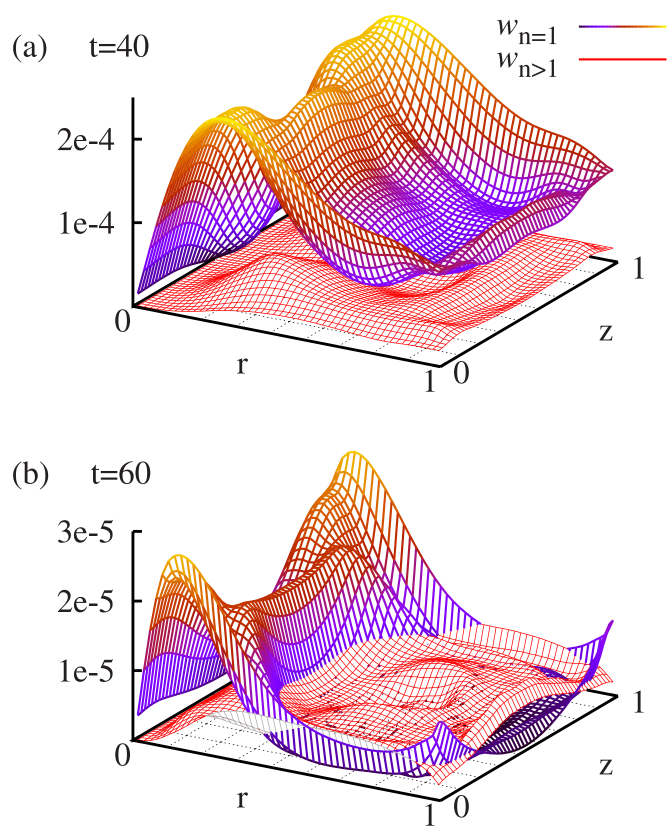

FIG. 10. (Color online) Magnetic energy density of the $n>0$ modes for the $\alpha=-0.7$, $S=814$ case during instability saturation (a) and at the beginning of the period of low activity (b).

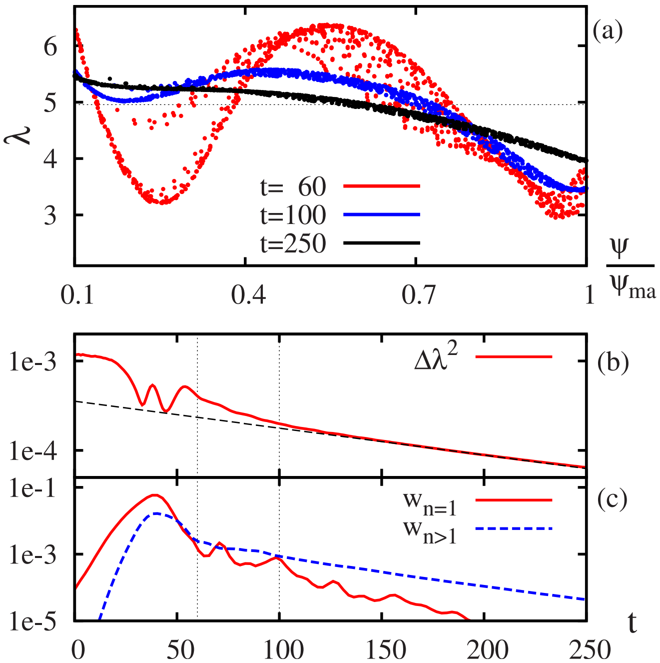

FIG. 11. (Color online) λ profiles for the $\alpha=-0.7$, $S=814$ case at several times (a). Integral of $\Delta\lambda^2=(\lambda-\lambda_1)^2$ in the annulus (b). Energy of the $n=1$ and $n>1$ modes in the annulus (c).

occur during this early period of time, for example, the rapid decay of magnetic energy, relative to helicity (Fig. 5). Nevertheless, the relaxation process does not finish with the instability saturation. Consider, for example, the case $\alpha=-0.7$ at $t=60$. Despite the fact that the flux amplification has finished [Fig. 4(b)] and the magnetic energy has been decaying almost at the same rate as the helicity during $20\tau_A$ (Fig. 5), the energy decay rate of the configuration [Fig. 6(b)] and its $\lambda(\psi)$ profile [Fig. 8(b)] are still far from their final values. We will see that the relaxation process finishes with a current redistribution process, produced by a small amount of MHD activity, which flattens the $\lambda(\psi)$ profile, and lasts several tens of Alfvén times ($\sim 40\tau_A$, in the $\alpha=-0.7$ case).

The magnetic energy density of the $n>0$ modes, in the poloidal plane, during instability saturation ($t=40$), is shown in Fig. 10(a) (for the $\alpha=-0.7$, $S=814$ case). As expected, the $n=1$ mode is dominant and it is mainly concentrated near the geometric axis. At $t=60$, when most of the activity has disappeared, the $n>1$ activity becomes dominant in the annulus [those points in the poloidal plane with $\tilde{\psi}>0.5$, see the contours in Fig. 15(a)]. From $t=60$ to $t=100$, a current redistribution process that flattens the λ profile (of the $n=0$ component of the solution) takes place [Fig. 11(a)]. Figure 11(b) shows the evolution of $\Delta\lambda^2=\int_{V_a}[\lambda(\mathbf{r})-\lambda_1]^2 d\mathbf{r}$, where V_a is the volume of the annulus. This quantity measures how far is λ from the λ_1 of the relaxed configuration, in the annulus. For large times, $t\gtrsim 100$, the exponential decay of this quantity, due to the action of resistivity, is observed. Before $t\sim 100$, the evolution toward a uniform λ profile is faster than that produced by the resistive processes due to the action of MHD activity. In particular, from $t=60$ to $t=100$, the action of the remaining MHD activity is still important, in spite of its small value. This is the final stage of the relaxation process induced by the instability. On the other hand, we note that during this current redistribution process, the $n=1$ mode is no longer dominant in the annulus [Fig. 11(c)].

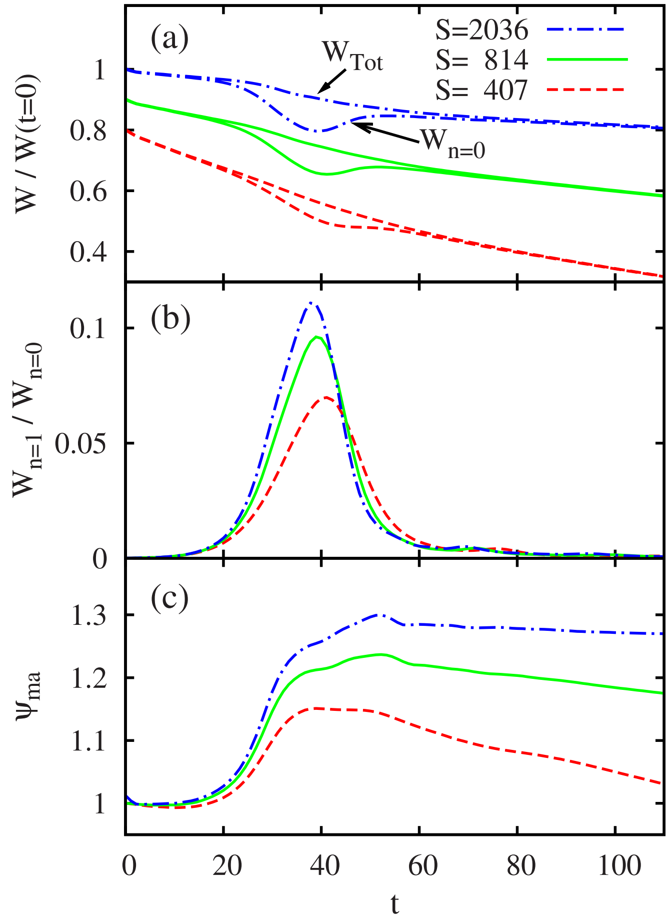

FIG. 12. (Color online) Total and $n=0$ magnetic energy (a), magnetic energy of the $n=1$ mode (b), and poloidal flux (c) evolutions for the $\alpha=-0.7$ case and different values of S.

C. Effect of resistivity

The results shown in Fig. 12, for $\alpha=-0.7$ and variable S, agree with the well know behavior[15] that when the resistive dissipation is decreased, more nonaxisymmetric activity is present, as a result of the instability, and higher flux amplification takes place. The following question arises: Does the partial relaxation process, described in Sec. III A, occur because the resistive dissipation limits the MHD activity responsible for relaxation? Although a simulation without resistivity is not available, the existing evidence indicates that this is not the case. First, the marked differences observed in the evolution for different values of S in Fig. 12 almost disappear when the decay of energy relative to helicity is considered (Fig. 13). The relation between these two quantities is indeed a good measure of the level of relaxation and Fig. 13 indicates that this level is controlled by the initial slope α and is independent of the Lundquist number S (at least for the relatively high S values considered here).

As pointed out in Sec. III B, the relaxation process does not finish immediately after the reduction in the ratio W/K. The evolution of the $\lambda(\psi)$ profile for two values of S is

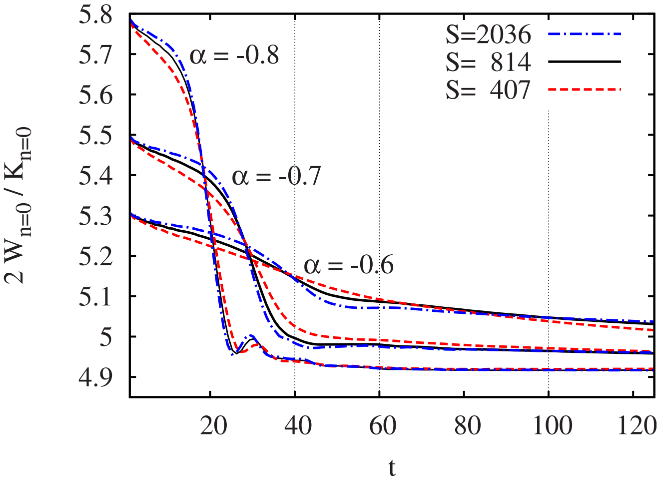

FIG. 13. (Color online) The same data as in Fig. 5 but considering different S values.

shown in Fig. 14 (for the $\alpha=-0.7$ case). At $t=60$, Fig. 14(a), the $\lambda(\psi)$ profiles are highly nonuniform, specially in the case with higher S, in which stronger activity has taken place. As discussed in Sec. III B, after $t=60$, a low activity period arises (the final stage of the relaxation event), in which the fluctuations produce a significant current redistribution that flattens the λ profile. It can be observed, in Fig. 14(b), that after this period the λ profiles are almost identical for the two cases with different S. This indicates that the λ uniformization produced by the relaxation event is independent of the Lundquist number (at large enough values of S). The curves shown in Fig. 14(b) correspond to the $\lambda(\psi)$ profiles when the action of the MHD fluctuations has just ceased. The effect of resistive dissipation, on these profiles, over $\sim 100\tau_A$ can be observed in Fig. 14(c).

D. Dynamo effect

The parallel component of the MHD dynamo field is usually expressed as $E_{d\parallel}=\langle \mathbf{v}\times\mathbf{b}\rangle\cdot\mathbf{B}/B$,[12] where $\mathbf{v}$ and $\mathbf{b}$ are the fluctuating parts of the velocity and magnetic field in the plasma, $\mathbf{B}$ is the mean field, and $\langle\cdot\rangle$ denotes temporal average. Our simulations are not in a steady sustained state, so we replace the time averaging by toroidal averaging. The nonaxisymmetric components of the solution are considered as the fluctuations and the mean magnetic field is the $n=0$ component of the total magnetic field. Figure 15(a) shows the time integrated value (from $t=0$ until $E_{d\parallel}$ vanishes, $t\sim 100$) of this quantity, in the poloidal plane, for the $\alpha=-0.7$, $S=814$ case. The temporal evolution of $E_{d\parallel}$ (multiplied by the radial coordinate) in five points at different positions in the poloidal plane are shown in Fig. 15(b). The positions of these points are indicated in Fig. 15(a). An antidynamo field in the outer flux surfaces near the geometric axis and a dynamo field in the inner flux surfaces is observed. This process is responsible for the flux amplification [Fig. 12(c)] and the toroidal current drive (Fig. 9) observed in the interval $20<t<40$.

The temporal evolution of $E_{d\parallel}^{\mathrm{ma}}$, i.e., $E_{d\parallel}$ at the magnetic axis $(r=0.62,\ z=0.5)$ is shown in Fig. 16(a). Substantial dynamo effect, which is the actual flux amplification mechanism, occurs during the linear phase of the instability $(t<40)$ and almost disappears at saturation $(t\sim 40)$. After that, smaller damped oscillations are present. For high S values, these oscillations may produce observable poloidal flux amplification, as observed in Fig. 12(c). In Fig. 16(b), the $E_{d\parallel}^{\mathrm{ma}}$ due to the $n>1$ modes is plotted. Note that the same y-axis scale than in (a) is employed. An important contribution from the $n>1$ activity, which grows rapidly with S, can be appreciated. In the curves of Fig. 16(a) this contribution was compensated by the $n=1$ component.

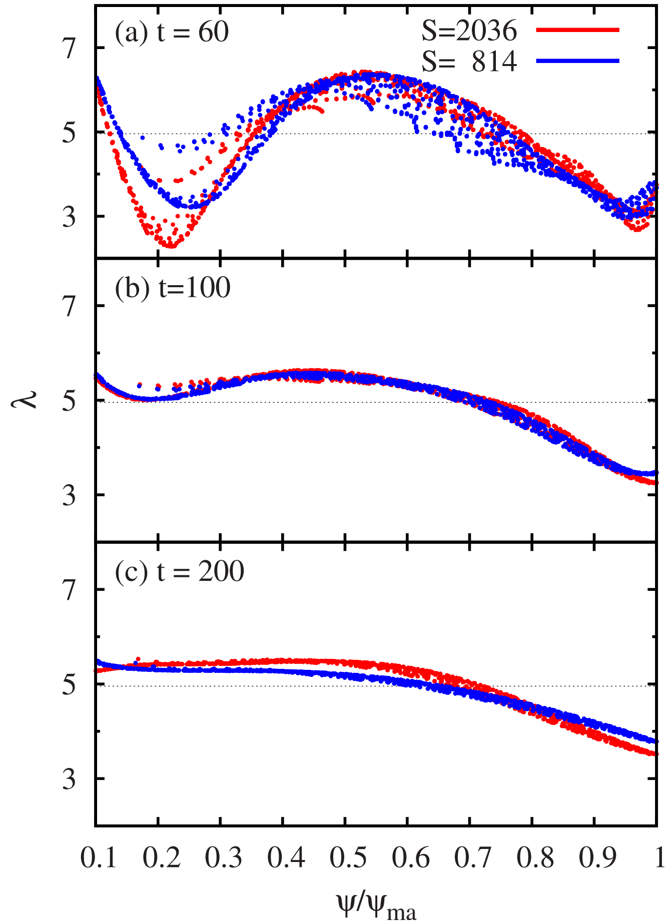

FIG. 14. (Color online) Comparison of the $\lambda(\tilde{\psi})$ profiles for the $\alpha=-0.7$ case at several times for two values of S.

The relaxation process, triggered by the kink instability of the central column of the spheromaklike configurations considered here, produces the desired effects of poloidal flux amplification and toroidal current drive at the cost of the presence of nonaxisymmetric disturbances, which degrade the quality of the flux surfaces and the confinement. A crucial point in spheromak research is to determine whether it is possible to drive toroidal current with a sufficiently low level of $n>0$ activity. In the context of the resistive MHD model, the parallel dynamo field is responsible for the current drive within the annulus. In Fig. 17 we plot, for each S, the maximum $E_{d\parallel}^{\mathrm{ma}}$ value versus the maximum $W_{n=1}/W_{n=0}$ value, obtained for different initial slopes α, ranging from -0.6 to -0.9. We consider the $\max(E_{d\parallel}^{\mathrm{ma}})$ value as a parallel dynamo level and the $\max(W_{n=1}/W_{n=0})$ value as a fluctuations level.

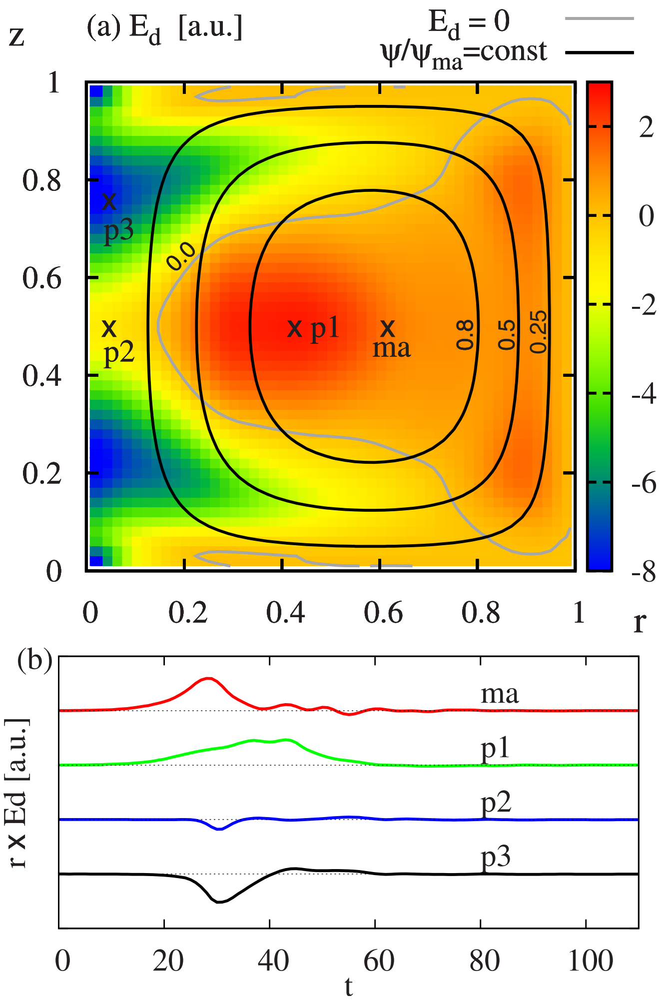

FIG. 15. (Color online) Time integrated value of $E_{d\parallel}$ in the poloidal plane, for the $\alpha=-0.7$, $S=814$ case (a). The gray contour ($E_{d\parallel}=0$) separates dynamo from antidynamo regions. Contours of $\tilde{\psi}$ at $t=0$ are also shown (black lines). Time evolution of $E_{d\parallel}$ times the radial coordinate, in the four points indicated in (a), are shown in (b).

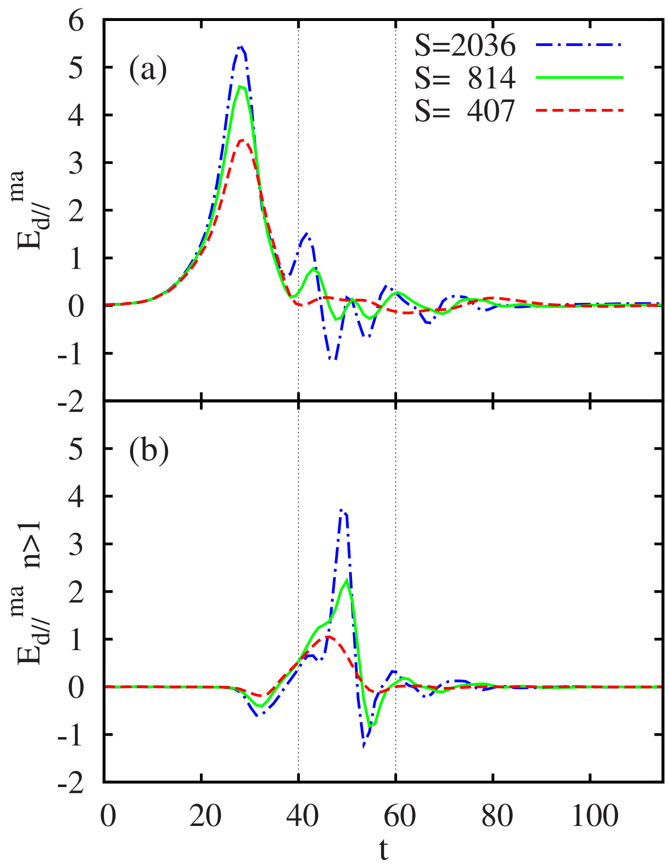

FIG. 16. (Color online) Evolution of $E_{d\parallel}$ at the magnetic axis ($r=0.62$, $z=0.5$), for different S values (a). When the contribution of the $n=1$ mode is removed, the curves shown in (b) are obtained.

As expected, a lower fluctuation level leads to a lower dynamo action, in all cases. On the other hand, it turns out that the dynamo level depends directly on the fluctuation level, regardless of which combination of α and S was employed to obtain that fluctuation level. In particular, an implication to the sustainment of a configuration against resistive dissipation is that when the resistivity decreases (higher plasma temperature), so less dynamo action is required, the necessary level of fluctuations will also decrease, since they are proportional to the dynamo, regardless of the Lundquist number.

IV. SUMMARY AND CONCLUSIONS

We studied the nonlinear evolution of several force-free equilibria inside a cylindrical flux conserver using the resistive MHD model. Each equilibrium was characterized by the slope α of its linear $\lambda(\psi)$ profile. In agreement with previous linear MHD stability results,[13] the configuration becomes unstable to the kink mode at $\alpha=-0.4$. We showed that, in order to correctly reproduce the initial linear phase of the instability in marginally unstable cases, it is necessary to perturb the equilibrium with the appropriate eigenmode. We described a simple technique to obtain a suitable numerical approximation of the kink eigenmode (for each α).

In the unstable cases, the kink instability triggers the magnetic relaxation process, which begins with the exponential growth of the $n=1$ kink mode, followed by the nonlinear saturation of the instability, and finishes with a low activity period. We compared the final states, achieved after the relaxation of unstable cases having different initial slopes α (and in consequence, different instability growth rates) with the minimum energy state allowed by our code (which has been shown to be almost identical to the Taylor state). In particular, the W/K ratio, the W decay rate, the B_θ and B_z radial profiles, and the $\lambda(\psi)$ profile, were analyzed in the comparison. We found that relaxation theory strictly applies only to very unstable cases ($\alpha\leq-0.8$). In contrast, the marginally unstable cases undergo a partial relaxation process. The level of relaxation produced by the instability (measured in terms of the W/K value, the W decay rate, and how far from uniform is the final λ profile) is proportional to how unstable the initial equilibrium is (indicated by α, where $\alpha=-0.4$ does not show any relaxation and $\alpha=-0.8$ leads to complete relaxation). While it is common to regard the partially relaxed profiles observed in experiments as the result of a competing process between sustainment and relaxation, here we showed that partial relaxation may occur even in the

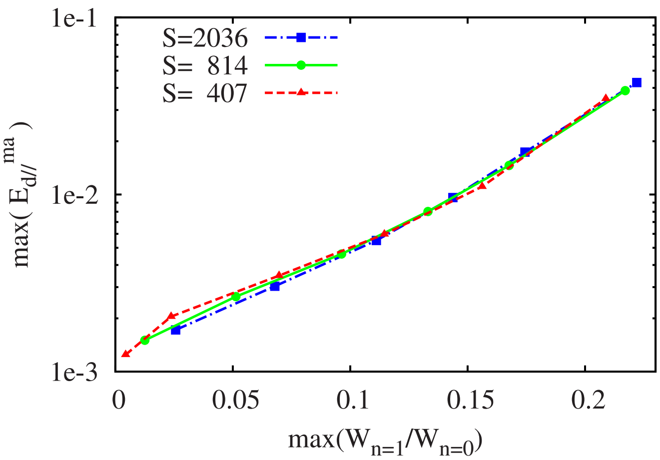

FIG. 17. (Color online) Maximum dynamo effect, $E_{d\parallel}^{ma}$, vs maximum fluctuation level, $W_{n=1}/W_{n=0}$, obtained for the different α values considered (from -0.6 to -0.9). The plot is repeated for each value of S.

absence of open field lines and sustainment, as a result of the dynamics of marginally unstable configurations.

We observed that the poloidal flux amplification is produced when the $n=1$ kink mode is dominant, few Alfvén times before nonlinear saturation. This is consistent with the experimental observation of the kink being the source of poloidal flux amplification.[11] At that time, the energy density of the instability is localized near the geometric axis. After saturation, the fluctuations decay fast, but they do not disappear. We showed that before the full recovery of axisymmetry, a low activity period takes place. This is the final stage of the relaxation event. During this period the MHD activity, remaining from the instability, produces a current redistribution process that flattens the λ profile. In contrast with the initial stage when poloidal flux is amplified, the $n=1$ mode is no longer dominant everywhere during this period. In particular, the energy of the $n>1$ modes in the annulus region (those flux surfaces with $\psi/\psi_{ma}>0.5$) is higher than the energy of the $n=1$ mode. Therefore, we conclude that, while the $n=1$ kink mode is dominant at the beginning of the relaxation event, when the poloidal flux is amplified and the energy decays rapidly relative to helicity, higher mode activity plays an important role (at least in the annulus) in the last stage of relaxation, which consist in the flattening of the λ profile.

We studied the effect of resistivity in the relaxation process, varying the Lundquist number S of the simulations over a moderate range. For a given initial slope ($\alpha=-0.7$), we found, as expected, that both the nonaxisymmetric activity and the flux amplification increase with S. However, we showed that even when stronger activity takes place, at higher S, the level of relaxation (in terms of the W/K ratio and the λ profile) of the final configuration remains unchanged (note that we considered high S values). This implies that, at high Lundquist numbers, the final relaxation level depends only on the initial slope α. We believe that these results, based on the nonlinear dynamics of the system, are relevant for devices sustained by helicity injection, since they operate around the stability boundary, at high Lundquist numbers. In order to obtain a better approximation to the actual process, one should incorporate the effect of field lines intercepting the boundary, which is a common feature of these devices. Besides, we expect relaxation in real plasmas to occur closer to the stability boundary than the case analyzed in more detail in this work (the $\alpha=-0.7$ case). The simulation of less unstable cases becomes more difficult because the dynamics is slower and the effects of resistivity become more important. The study of less unstable cases with open field lines at higher Lundquist numbers should be the next step.

We computed the time average, over the whole relaxation event, of the dynamo field in the poloidal plane. An antidynamo process in the outer flux surfaces, near the geometric axis, and a positive dynamo in the inner flux surfaces, surrounding the magnetic axis, are observed. The toroidal component of the dynamo field at the magnetic axis rises rapidly with the growth of the kink stability, reaches its maximum, and decreases almost to zero just before the instability saturation. We showed that this peak (which is directly responsible for poloidal flux amplification, through Faraday's law) is produced by the $n=1$ component of the fluctuations. After saturation, higher mode fluctuations produce a significant contribution to the dynamo, which is compensated by the $n=1$ component, in such a way that little flux amplification takes place after saturation. The amplitude of this contribution grows rapidly with S. We observed that the maximum dynamo at the magnetic axis grows rapidly with the maximum fluctuation level (the $W_{n=1}/W_{n=0}$ at saturation) developed during the instability. We also observed that a given dynamo level is produced by a given fluctuation level, regardless which combination of α and S produced that level (note that the fluctuation level produced by an equilibrium with a given α is modified when S is varied, thus the same level of fluctuations may be achieved with different α values). In the context of devices sustained by the MHD dynamo action, this implies that if S is increased, so less dynamo action is required, a lower fluctuation level will be necessary in order to sustain the configuration.

ACKNOWLEDGMENTS

The authors would like to acknowledge financial support from Universidad Nacional de Cuyo (Argentina), the Agencia Nacional de Promoción Científica y Tecnológica (ANPCyT), and CONICET (Argentina).

[1] T. R. Jarboe, Plasma Phys. Controlled Fusion **36**, 945 (1994).
[2] P. M. Bellan, *Spheromaks* (Imperial College Press, London, 2000).
[3] J. B. Taylor, Phys. Rev. Lett. **33**, 1139 (1974).
[4] J. B. Taylor, Rev. Mod. Phys. **58**, 741 (1986).
[5] S. O. Knox, C. W. Barnes, G. J. Marklin, T. R. Jarboe, I. Henins, H. W. Hoida, and B. L. Wright, Phys. Rev. Lett. **56**, 842 (1986).
[6] P. K. Browning, G. Cunningham, S. J. Gee, K. J. Gibson, A. Al-Karkhy, D. A. Kitson, R. Martin, and M. G. Rusbridge, Phys. Rev. Lett. **68**, 1718 (1992).
[7] E. B. Hooper, L. D. Pearlstein, and R. H. Bulmer, Nucl. Fusion **39**, 863 (1999).
[8] D. M. Willett, P. K. Browning, S. Woodruff, and K. J. Gibson, Plasma Phys. Controlled Fusion **41**, 595 (1999).
[9] D. P. Brennan, P. K. Browning, and R. A. M. van der Linden, Phys. Plasmas **9**, 3526 (2002).

[10]R. C. Duck, P. K. Browning, G. Cunningham, S. J. Gee, A. al-Karkhy, R. Martin, and M. G. Rusbridge, Plasma Phys. Controlled Fusion **39**, 715 (1997).
[11]S. C. Hsu and P. M. Bellan, Phys. Rev. Lett. **90**, 215002 (2003); e-print arXiv:physics/0304104v2.
[12]A. Al-Karkhy, P. K. Browning, G. Cunningham, S. J. Gee, and M. G. Rusbridge, Phys. Rev. Lett. **70**, 1814 (1993).
[13]U. Shumlak and T. R. Jarboe, Phys. Plasmas **6**, 4382 (1999).
[14]K. Katayama and M. Katsurai, Phys. Fluids **29**, 1939 (1986).
[15]V. A. Izzo and T. R. Jarboe, Phys. Plasmas **10**, 2903 (2003).
[16]C. R. Sovinec, J. M. Finn, and D. Del-Castillo-Negrete, Phys. Plasmas **8**, 475 (2001).
[17]G. Tóth, Astrophys. Lett. Commun. **34**, 245 (1996) (http://www.astro.uu.nl/toth/).
[18]G. Tóth, J. Comput. Phys. **161**, 605 (2000).
[19]H. Forrer and R. Jeltsch, J. Comput. Phys. **140**, 259 (1998).
[20]D. A. Kitson and P. K. Browning, Plasma Phys. Controlled Fusion **32**, 1265 (1990).